13th ewtec 2019 Proceedings of the 13th European Wave and Tidal Energy Conference 1-6 Sept 2019, Naples, Italy

On the Effect of elastic Blade Deformation on the Performance of a horizontal Axis Tidal Current Turbine

Nicholas Kaufmann, Thomas H. Carolus, and Ralf Starzmann

Abstract— **During the model scale testing of a newly designed 6.3 m horizontal axis fixed-pitch tidal turbine, a distinct - undesired - deformation of the 1:12.6 brass model was observed. The objective of this contribution is a numerical and experimental assessment of a potential performance modification due to the observed deformation.**

To simulate the bending and twisting an extended and validated blade element momentum (BEM) model, predicting the turbine performance including the cavitation characteristics, was coupled to the finite element method (FEM) solver from ANSYS Mechanicals®.

The deformation was predicted for a wide operating range utilizing the BEM-FEM coupling. It was found that the axial bending of the blades was accompanied by a distinctive torsion which led to increased pitch angels. Comparing the performance predictions for the rigid and flexible rotor blades showed that the obtained variation in pitch angle distribution led to i) a decreased power output, ii) reduced thrust loads and iii) somewhat lower critical cavitation numbers.

Experimental performance characteristics of the - unavoidably flexible - model scale turbine were obtained in comprehensive towing tank and cavitation tunnel tests. A comparison with the prediction strongly suggests, that the model-scale turbine experienced the performance changing deformation as simulated from the FEM model.

Keywords— **BEM-FEM Coupling, Fluid-Structure-Interaction, Horizontal Axis Tidal Current Turbine, Model-Scale Testing**

I. Introduction

An elastic deformation of the blades of modern small tidal turbines with blades manufactured from composites is unavoidable and even used to control their performance. As examples, the rotor design of the horizontal axis fixed-pitch SIT250 turbine and its predecessor STG50 from SCHOTTEL HYDRO purposefully aims for an elastic deformation – in particular torsion – to reduce the thrust loads in off-design conditions (cp. [1] and [2]). The full-scale testing of the 4 m diameter STG50 turbine showed a significant decrease of the thrust due to the elastic deformation of the blades [3].

In the first model scale tests of a new turbine, however, rigid rotor blades are preferred as these tests aim for a validation of the principle hydrodynamic rotor performance. Geometrical restrictions of the test facilities limit the size of the scaled model turbines and lead to thin rotor blades. Thus, due to the delicacy of model turbines undesired blade deformation cannot be excluded.

Axial bending, i.e. in direction of the ingested inflow, may have a minor impact, but torsion around the radial axis and the thus effect of a variation of pitch angle distribution is seen of utmost relevance. For given operating conditions, i.e. flow angle β_∞, a change of the pitch angle γ at a blade cross section causes an alteration of same magnitude of the angle of attack α:

$$\alpha = \beta_\infty - \gamma \tag{1}$$

Fig. 1 schematically shows the effect of a pitch angle variation $\Delta\gamma$ on the lift force F_L and drag force F_D. Increasing γ by $+\Delta\gamma$ ("pitch to feather") causes a decrease of α, resulting in a reduced lift force F_L. On the other hand, decreasing the pitch angle by $-\Delta\gamma$ increases the angle of attack, resulting in a higher lift force up to the stall point (pitch to stall). Furthermore, the higher α cause increased drag forces F_D. Introducing the normal and tangential forces per unite span,

$$F_n = F_L \cos(\beta_\infty) + F_D \sin(\beta_\infty) \tag{2}$$

and

$$F_t = F_L \sin(\beta_\infty) - F_D \cos(\beta_\infty) \tag{3}$$

the *rotor shaft power* P and *rotor axial force* F_{ax} (i.e. thrust T) result from a spanwise integration from hub to tip and a multiplication with the number of the blades N_B and the angular velocity of the rotor Ω:

ID: 1403 11-05 Submission Track: TDD.

This work was founded by the Federal Ministry for Economic Affairs and Energy of Germany (BMWi) within the project TIDAL POWER (FKZ: 0325817B)

N. Kaufmann was with the Institute of Fluid- and Thermodynamics, University of Siegen, 57068 Siegen, Germany. He is now at SCHOTTEL HYDRO GmbH, Mainzer Str. 99, 56322 Spay, Germany.

T. H. Carolus is with the Institute of Fluid- and Thermodynamics, University of Siegen, 57068 Siegen, Germany.

R. Starzmann is with SCHOTTEL HYDRO GmbH, Mainzer Str. 99, 56322 Spay, Germany.

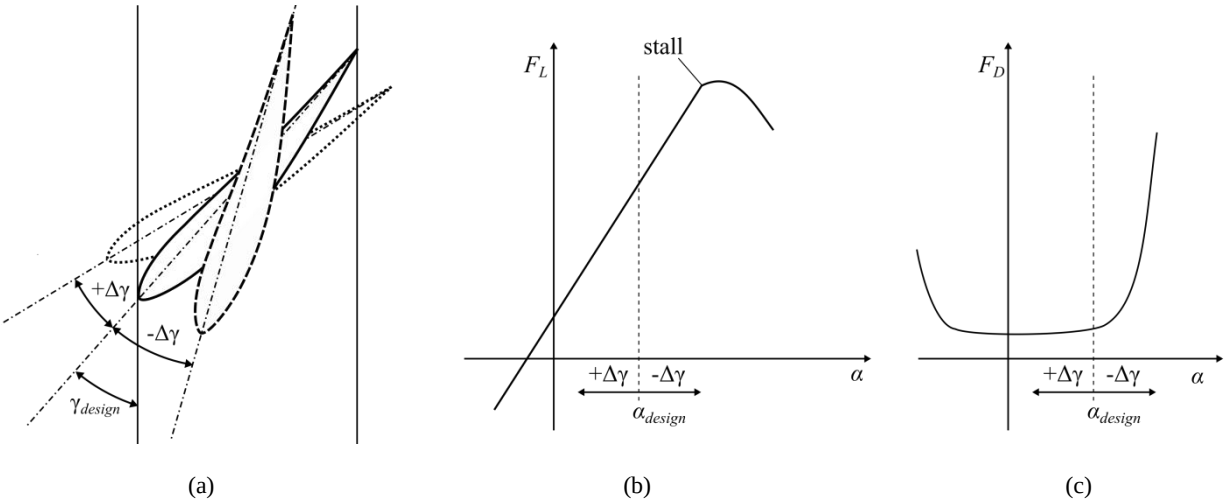

(a) (b) (c)

Fig. 1 Pitch angle variation: (a) design pitch (solid), pitch to feather (dotted) and pitch to stall (dashed); (b) effect of pitch variation on the angle of attack α and hydrodynamic lift and drag force F_L and F_D (c), respectively.

$$F_{ax} = T = N_B \int_{r_{hub}}^{r_{tip}} F_n(r)dr \tag{4}$$

and

$$P = M\Omega = N_B \int_{r_{hub}}^{r_{tip}} F_t(r) r dr, \tag{5}$$

respectively. Thus, pitch-to-feather is expected to reduce the P and T whereas pitch-to-stall is most likely causing increasing thrust until stall and increasing P as long as the increased lift is not compensated by the raising drag (cp. e.g. [4]).

The majority of the literature discussing the effect of blade deformation on the performance of horizontal axis tidal turbines is focusing of blades made from fiber reinforced composite materials. For example, NICHOLLS-LEE et al. presented in [5] the numerically investigation of the performance of a 20 m diameter three-bladed horizontal axis tidal current turbine. The structural design concept of the rotor utilizes the *bent-twist* coupling of composite materials to enable load related torsion of the blades. They coupled a blade-element-momentum model (BEM) with a finite-element model (FEM) to predict the load related deformation of the blades as well as the corresponding changes of the turbine performance. Their results indicated a reduction of the axial loads of up to 10% while increasing the annual energy production in an example case up to 5%. MOTLEY and BARBER varied in [6] the orientation of the fibers within the blades' composite to obtain a pitch-to-feather as well as a pitch-to-stall torsion, respectively, from the same blade shape. Thus, for this example solely the nonhomogenous material properties determine the load related torsion of the blades. They used a 3D potential-based boundary element method coupled to a FEM solver as fluid-structure-interaction tool to estimate the blade deformation and performance. Their results showed that an increased power capture is accompanied by increased thrust loads (pitch-to-stall case) whereas the pitch-to-feather configuration yielded a reduced power output but also reduced thrust loads. In [7] BARBER et al. presented the experimental results of flume testing proving that different fiber orientations enable pitch-to-stall as well as pitch-to-feather behavior for a single blade shape. MURRAY et al. developed a FSI tool which utilizes a BEM model coupled to a FEM model to design a blade for a 1:20 scale model of a horizontal axis tidal turbine from composite material [8]. The load-related deformation of the blade let to decreased power (5%) and thrust (6%) for the maximum flow speed at the simulated site. By applying a pretwist to the blade they compensated the deformation at the design conditions such that the power capture was the same as for the initial - rigid – blade geometry at this particular operating point. In [9] MURRAY et al. compared the experimentally obtained performance of a "flexible" composite rotor to a "rigid" rotor manufactured from aluminum. The results showed a significant reduction of power and thrust for the composite blades.

The load related torsion of the studies above is attributed to the bent-twist behavior of the utilized composite materials. The objective of this contribution is to numerically model the deformation of the blades manufactured from brass, i.e. with isotropic properties. The aim is to examine whether the visually observed deformation of a scaled turbine model influenced the measurement results of towing tank and cavitation tunnel tests. Therefore, a BEM model is coupled to an FEM model and solved iteratively. The power, thrust and cavitation characteristics are predicted for the deformed blades as well as for the rigid rotor utilizing the BEM model. Finally, the predicted characteristics of the "flexible" and "rigid" turbine are compared against experimental results of the model scale tests.

II. INVESTIGATED TURBINE

The turbine investigated in this contribution is a 1:12.6 brass model of the horizontal axis fixed-pitch turbine for tidal currents, the SIT 250 by SCHOTTEL HYDRO, shown in **Fig. 2**. The SIT250 is designed as a modular turbine system utilizing one drivetrain and two rotor diameters, 4 m and 6.3 m, which can be selected based upon the varying velocity frequency distributions of different deployment sites. This work discusses the scaled model of the 6.3 m diameter rotor design. The model rotor is CNC-milled from brass by the workshop of the Schiffbauversuchsanstalt Potsdam (SVA) and hub is complemented with a plastic hull to replicate the full-scale geometry, as shown in **Fig. 2**.

The SIT250 drive train is rated at a mechanical shaft power of P_{rated} = 85 kW which corresponds to a grid ready power of P_{el} = 70 kW. The blades of the full-scale turbines are made from fiber-reinforced composite. The elasticity of these blades provides an additional load reduction at high inflow velocities ("passive-adaptive pitch") through an elastic pitch-to-feather behavior. A so called "overspeed" strategy by the speed controller limits the power output to rated power as described in KAUFMANN et al. [10]. Nevertheless, a mechanical brake is added to stop the turbine. A two stage planetary gearbox and an asynchronous generator complete the drive train. The turbine is manufactured by SCHOTTEL HYDRO, Germany.

Fig. 2 1:12.6 model of the 6.3 m rotor of the SIT250 tidal turbine utilized for the model tests.

Special attention was given to the hydraulic design of the turbine blades. A novel multi-objective optimizing scheme, described in [4], has been developed targeting the best compromise between maximum power output, minimum thrust load and shallowest immersion depth for operation without cavitation. To support the passive-adaptive pitching, the stacking line of the blade has been designed to provide a sufficient positive moment around the radial axis, so called *pitching moment Mz*, as described in [4].

III. FLUID-STRUCTURE-INTERACTION MODEL

A fluid-structure-interaction (FSI) model, schematically shown in Fig. 3, is utilized within for this work to predict the performance characteristics of horizontal free-flow turbines considering the load related deformation of the blades. The key components of the model are

- an extended performance prediction model based on the BEM theory
- a FEM solver (commercial software ANSYS Mechanical® of ANSYS® 18.2)

To initialize the simulation, the BEM model is used to predict the spanwise load distribution for a given operating point. The loads are applied to the FEM model which is solved to predict the deformation of the blade due to the acting loads. Subsequently, the induced torsion $\Delta\gamma_{el}$ along the blade span is calculated based on the displacements of specified points along the leading edge (LE) and trailing edge (TE), respectively. Considering the changed pitch angle distribution, the BEM model predicts the performance and the updated loads are passed to the FEM model to actualize the deformation. This iteration is repeated until the change of the pitch angle at the blade tip is less than 0.01% with respect of the previous iteration. Eventually, the power, thrust and cavitation characteristics are predicted for the chosen operating point by the BEM model utilizing the final pitch angle distribution.

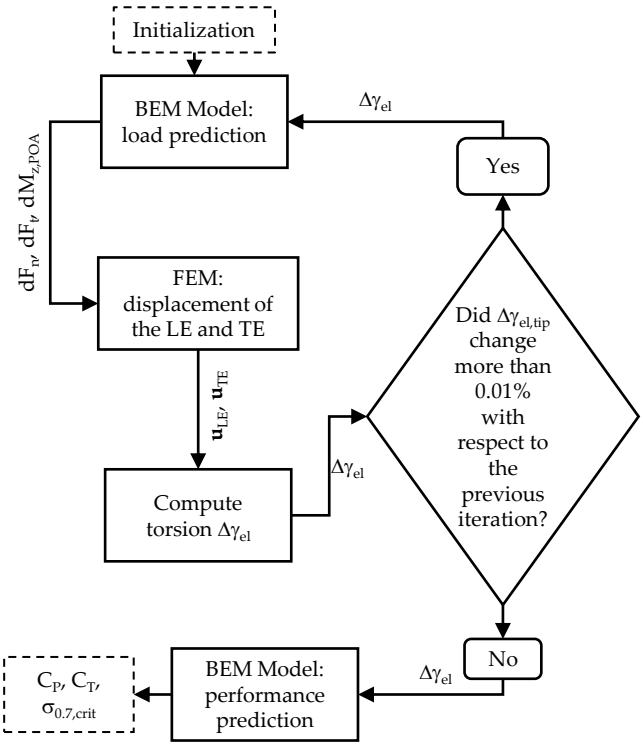

Fig. 3 Basic scheme of the coupled BEM-FEM model to predict the performance of turbines with flexible rotor blades

A. Performance Prediction Using BEM

Here we use an enhanced in-house BEM method - briefly summarized in the next paragraph - for the prediction of the performance and cavitation characteristics of a given turbine. A detailed description of the model as well as a validation based on model scale test data is given in KAUFMANN et al. [11].

It is common practice to describe the turbine performance in terms of the non-dimensional characteristics

- tip speed ratio

$$\lambda = \frac{r_{tip}\Omega}{U_0} \tag{6}$$

- power coefficient

$$C_P = \frac{P}{0.5\rho U_0^3 \pi r_{tip}^2} \tag{7}$$

- thrust coefficient

$$C_T = \frac{T}{0.5\rho U_0^2 \pi r_{tip}^2} \tag{8}$$

- cavitation number

$$\sigma_{0.7} = \frac{p_{atm} + \rho g h_{hub} - p_v}{0.5\,\rho U_0^2 (1 + (0.7\lambda)^2)} \tag{9}$$

U_0 is the free flow velocity far upstream of the turbine. ρ is the density and p_v the vapor pressure of the fluid, p_{atm} the atmospheric pressure, g the gravity and h_{hub} the immersion depth of the hub. Cavitation is avoided when the cavitation number exceeds a critical value $\sigma_{0.7,crit}$.

In spanwise direction the turbine blade is segmented into a number of blade elements (BE). For every BE, the local power and thrust coefficients are derived based on momentum conservation ($C_{P,M}$ and $C_{T,M}$) and the dynamic forces on a quasi 2D hydrofoil ($C_{P,DF}$ and $C_{T,DF}$). Equating $C_{P,M} = C_{P,DF}$ and $C_{T,M} = C_{T,DF}$ yields two nonlinear equations for the unknown local axial and tangential velocity components and eventually the BEs' C_P and C_T. The overall turbine performance at a specific tip speed ratio then results from a summation over all BEs.

Simplifying assumptions, such as a flow field that is purely 2D, are limiting the precision of the basic BEM theory. In order to increase the accuracy of the method, various sub-models are applied. B's [12] correction of the thrust coefficient for large axial flow retardation is used, furthermore models by PRANDTL/GLAUERT [13] and SHEN [14] accounting for blade hub and tip losses.

The hydrodynamic forces (lift and drag) for all BEs are needed to determine $C_{P,DF}$ and $C_{T,DF}$. Since lift and drag of the hydrofoil sections are functions of the Reynolds number Re and angle of attack α, they are calculated in advance and stored in a database. These polar data are obtained utilizing the public domain code XFOIL by DRELA [15]. To mimic an incompressible flow, the Mach number is set to zero. The transition from a laminar to turbulent boundary is calculated using the e^n-method with a threshold amplification ratio of $N_{crit} = 1$, which corresponds to a free stream turbulence level of 2% [16]. Post-stall data are extrapolated according to VITERNA et al. [17]. Although VITERNA's correlation is empirical and known for its limited accuracy, it ensures the needed numerical stability.

Cavitation in a turbine is a very complex phenomenon and affected by a variety of factors, which naturally cannot all be accounted for within a semi-analytic BEM method. The cavitation number $\sigma_{0.7}$ introduced in (9) is solely a function of the turbine's operating conditions, independent of the blade shape. However, cavitation is avoided when the cavitation number exceeds a critical value $\sigma_{0.7,crit}$. Thus, for each λ the value of $\sigma_{0.7}$, where cavitation inception is observed, is defined as $\sigma_{0.7,crit}$. For a given rotor geometry, the turbine's cavitation characteristic is given by $\sigma_{0.7,crit}(\lambda)$. It is usually determined experimentally in a cavitation tunnel by varying the static pressure. For designing or optimizing a rotor blade, the a priori prediction of $\sigma_{0.7,crit}$ (λ) is crucial. Cavitation may occur on the blade suction surface and near the blade tip region due to the presence of the tip vortex. Typically, the onset of tip vortex cavitation is prior to blade suction surface cavitation. The BEM model is not capable of predicting the tip vortex flow. However, since tip vortex cavitation does rarely harm the blade structure nor degrade the turbine performance, this limitation is accepted. Then, an estimate of the turbine cavitation characteristics can be made on the basis of the chordwise pressure distributions of the BEs which are linked to lift and drag. These pressure distributions are also taken from XFOIL, accepting that 3-D effects are not resolved. The aim of the implemented model is predicting the inception of cavitation in order to determine the turbine operating range free of cavitation as a function of design, placement below the free surface and inflow velocity to the rotor. A performance prediction of the cavitating turbine is by no means an outcome of the model.

B. FEM Model

The FEM model, i.e. description of the blade through mesh, specification of the load application and definition of the material properties, is done in advance utilizing the preprocessing tools included in the ANSYS® software package. Solely a single blade of the turbine is modeled within FEM analyses since the BEM model assumes uniform conditions across the rotor. The hub and the interface to the blade are not included in the FEM model. Instead, the blade is constrained in all degrees of freedom at the root. The blade is divided into sections based on the blade elements utilized within the BEM model. An automatic meshing application by ANSYS® is used aiming for a mesh of mainly hexahedral 3D elements supplemented with tetrahedral elements if necessary. The properties of

the applied isotropic linear elastic material correspond to the brass type (CuZn39Pb2 cp. [18]) of which the model turbines are milled from.

C. Integration to the Fluid-Structure-Interaction Model

The axial and tangential loads are applied in the FEM model at fixed points equivalent to the positions used within the BEM model, i.e. at 25% of the chord length from the LE, exemplarily shown for a blade cut in **Fig. 4.** The forces obtained from XFOIL refer to these points. An additional moment $M_{z,POA}$ accounts for the distance of this reference point to the true point of application. Thus, $M_{z,POA}$ acting on a BE is applied to the FEM model in addition to the normal and tangential force components.

The nodal displacements $\mathbf{u}_{LE,i}$ and $\mathbf{u}_{TE,i}$ of i points $\mathbf{P}_{LE,i}$ and $\mathbf{P}_{TE,i}$ along the LE and TE, respectively, resulting of the FEM analysis are used to determine the local elastic torsion $\Delta\gamma_{el,i}$ (cp. **Fig. 5**). Therefore, $\mathbf{u}_{LE,i}$ and $\mathbf{u}_{TE,i}$ are applied on points $\mathbf{P}_{LE,i}$ and $\mathbf{P}_{TE,i}$ of the undeformed blade to obtain the displaced points $\mathbf{P}'_{LE,i}$ and $\mathbf{P}'_{TE,i}$, as shown in **Fig. 5**. Eventually, the angle between the vectors connecting the LE and the TE, before and after the deformation, yields the local elastic torsion,

$$\Delta\gamma_{el,i} = \arccos\left(\frac{\langle \overline{P_{LE,i}P_{TE,i}} \circ \overline{P'_{LE,i}P'_{TE,i}} \rangle}{|\overline{P_{LE,i}P_{TE,i}}| \cdot |\overline{P'_{LE,i}P'_{TE,i}}|}\right). \quad (10)$$

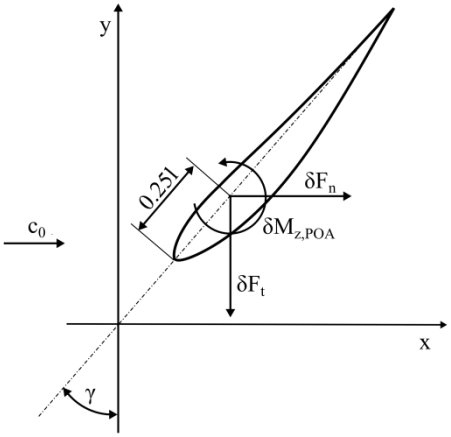

Fig. 4 Forces and loads applied to the FEM model for one cross-section (schematically).

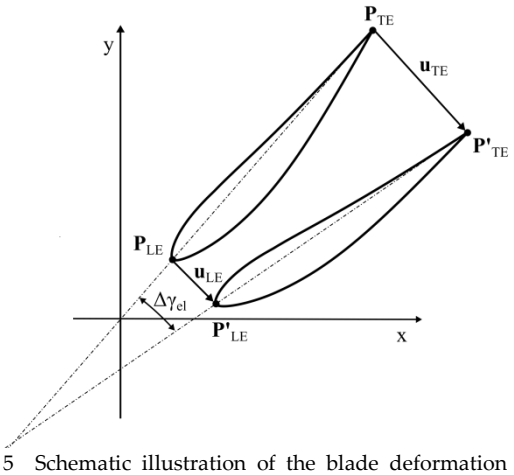

Fig. 5 Schematic illustration of the blade deformation at one cross-section.

IV. Experimental Setup

D. Towing Tank

The non-dimensional performance characteristics (C_P and C_T) of the model-scale turbine are measured in a towing tank, i.e. the turbine is dragged through a basin of calm water. Thus, the free-flow velocity far upstream U_0 corresponds to the speed of the towing vehicle. The experiments are performed at the ship model basin in Potsdam Germany, the Schiffbau-Versuchsanstalt Potsdam GmbH (SVA). The most relevant data of the utilized towing tank are compiled in Table I.

TABLE I
SVA TOWING TANK FACILITY

Towing tank dimensions	280.0 m length 9.0 m width 4.5 m depth
Maximum carriage velocity (corresponding to c_0)	7.0 m/s
Dynamometer type H39, Kempf and Remmers	n_{max} = 60 s^{-1} T_{max} = 1000 N Q_{max} = 50 Nm

Since the diameter of the model scale turbine is d_{tip} = 0.5 m, the resulting cross-sectional blockage of the open water tests is 0.5%. The shaft of the turbine is immersed more than one rotor diameter below the waterline and located downstream of the rotor to avoid interaction with the water surface and the wake of the shaft. **Fig. 6.2** depicts the towing tank setup.

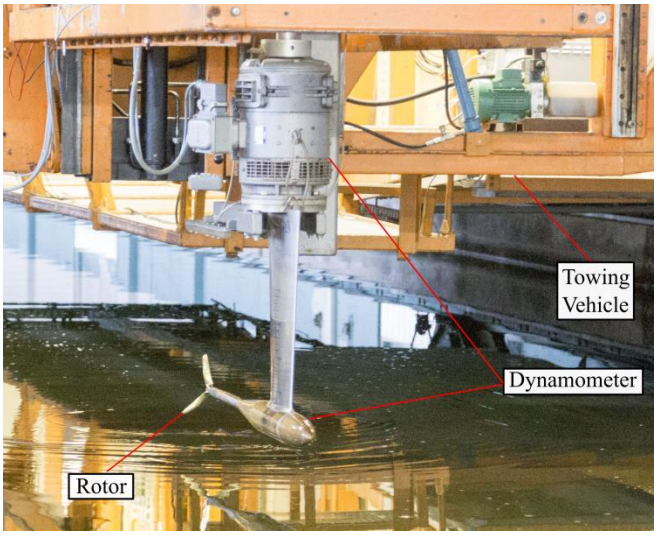

Fig. 6 SVA towing tank test rig in maintenance position.

The testing follows the recommendation of the International Towing Tank Conference (ITTC) for open water tests of scaled models [19]. Tests are carried out at different velocities and over a range of tip speed ratios, which is achieved by varying the rotational speed of the turbine for a given c_0. 10 s-time records of thrust, torque, rota-

tional speed and c_0 (towing vehicle speed) are captured synchronously. According to the recommendations of the ITTC [19], the measured values for thrust and torque are corrected by using a dummy hub having the same mass as the model turbine.

E. Cavitation Tunnel

For cavitation studies, the same turbine as for the towing tank tests is placed in the cavitation tunnel of the SVA with the specification as in **Table II**. The turbine is positioned in the measuring section ("test section") and the water is pumped around a closed-loop configuration (vertical) providing U_0 to the turbine.

The procedure of the testing follows the ITTC standards for cavitation tests [20]. Due to the high cross-sectional blockage ratio of 27%, a blockage correction has to be applied to match the operation points at free-flow conditions. The applied correction follows mainly the methodology presented by BAHAJ et al. in [21].

TABLE II
SVA TOWING TANK FACILITY

Cavitation tunnel test section (length)	2600 mm
Cavitation tunnel test section (cross-section)	850 mm x 850 mm
Pressure variation	-950 mbar – +1200 mbar
Maximum flow velocity (corresponding to U_0)	7.5 m/s
Dynamometer H36, Kempf and Remmers	n_{max} = 60 s^{-1} T_{max} = 2000 N Q_{max} = 100 Nm

To determine the critical cavitation number, an operating point in terms of U_0 and n (i.e. λ) is kept constant and the static pressure in the cavitation tunnel is decreased continuously starting in non-cavitating conditions. As soon as cavitation is observed the conditions are locked up and applied to (9) to obtain corresponding and hence critical cavitation number. A quasi-static visualization of the rotor is obtained through stroboscope providing a flash-light according to the rotational speed.

V. NUMERICAL RESULTS

In **Fig. 7** the simulated spanwise displacement of the LE in x and y direction (*axial* and *circumferential* cp. coordinate system in **Fig. 4**) as well as the change of the pitch angle $\Delta\gamma_{el}$ are shown for λ = 6 and increasing U_0. As expected is the axial deflection (in x-direction) substantially larger as compared to the circumferential displacement. In both cases, the deflection increases from the blade root to tip and with increasing values of U_0. Besides the axial and circumferential displacements, the simulations resulted in an additional torsion of the blades. Interestingly, $\Delta\gamma_{el}$ is negative (i.e. pitch to stall) at the blade root region before increasing to the maximum $\Delta\gamma_{el}$ at the tip. However, for the majority of the blade the torsion increases for faster inflow velocities U_0 resulting in larger pitch angles.

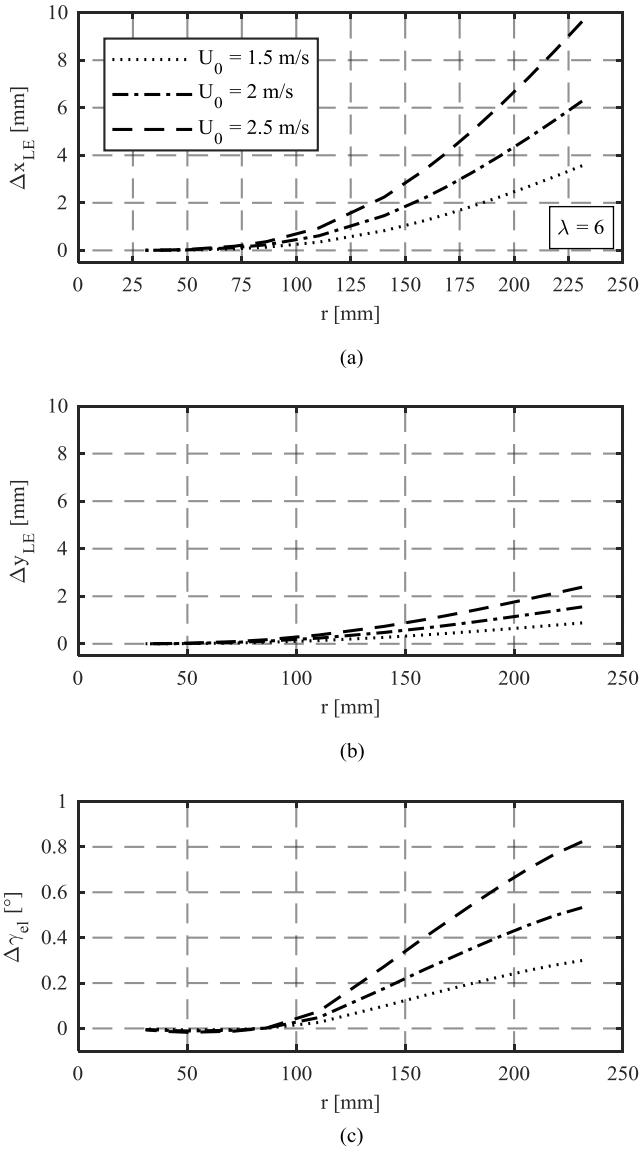

Fig. 7 Simulated deformation along the blade at the design point λ = 6 for varying inflow velocities: (a) axial displacement of the LE; (b) tangential displacement of the LE; (c) and the induced pitch angle $\Delta\gamma_{el}$.

The simulated displacement of the blade tip as function of the tip speed ratio is shown in **Fig. 8** for three different U_0. As for the results at the design point, presented in **Fig. 7**, the deflection and torsion of the blade increases with the U_0. However, the axial and circumferential deflection decreases for high tip speed ratios whereas the induced pitch angle further rises. As shown in **Fig. 9** this might be due to the rising values of the pitching moment $M_{z,POA}$. F_t and F_n decrease for high tip speed ratios whereas the maximum values of $M_{z,POA}$ are at the highest λ simulated. A possible explanation is that the true point of application of the resulting force moves towards the TE the higher the tip speed ratio. Thus, even though the magnitude of the resulting force decreases, M_z further increases due to the larger lever.

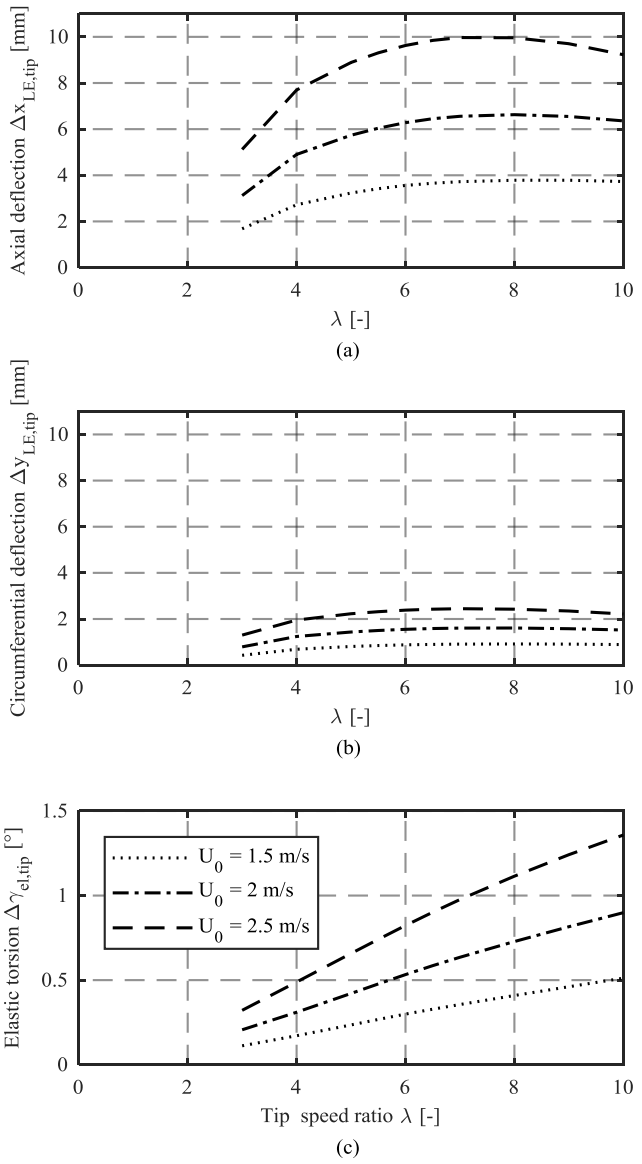

Fig. 8 Simulated deflection at the blade tip as function of the tip speed ratio for varying inflow velocities: (a) axial displacement of the LE; (b) circumferential displacement of the LE; (c) induced pitch at the blade tip.

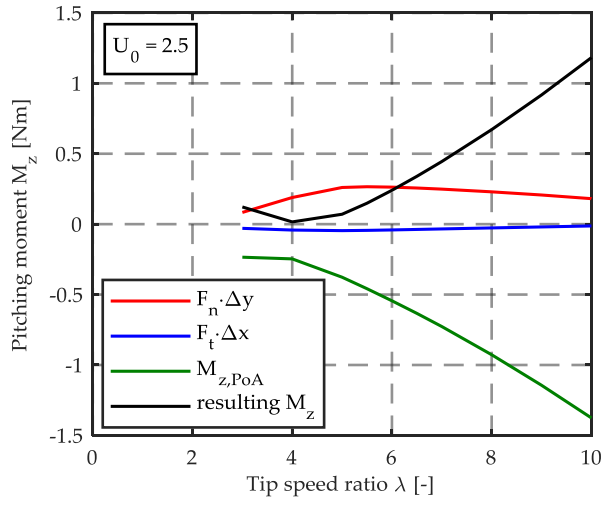

Fig. 9 Pitching moments resulting from axial force, tangential force and distance of the reference point POA to the true point of application ($M_{z,POA}$) for U_0= 2.5 m/s as function of the tip speed ratio.

The influence of the blade deformation on the predicted turbine performance is shown in **Fig. 10**. The induced pitch angles result in lower power and thrust values. Increasing $\Delta\gamma_{el,}$, either through higher U_0 or higher λ, lead to a significant reduction of C_P and C_T. Thus, the deformation acts as a kind passive "pitch to feather" control even for blades from brass with isotropic material properties. As for the power and thrust, the reduction of $\sigma_{0.7,crit}$ increases with λ but after a critical tip speed ratio the difference decreases for higher λ. At λ = 10 the flexible rotor has even higher $\sigma_{0.7,crit}$. This is most likely due to cavitation on the blades pressure side which occurs at low α and hence is more likely for the deformed rotor.

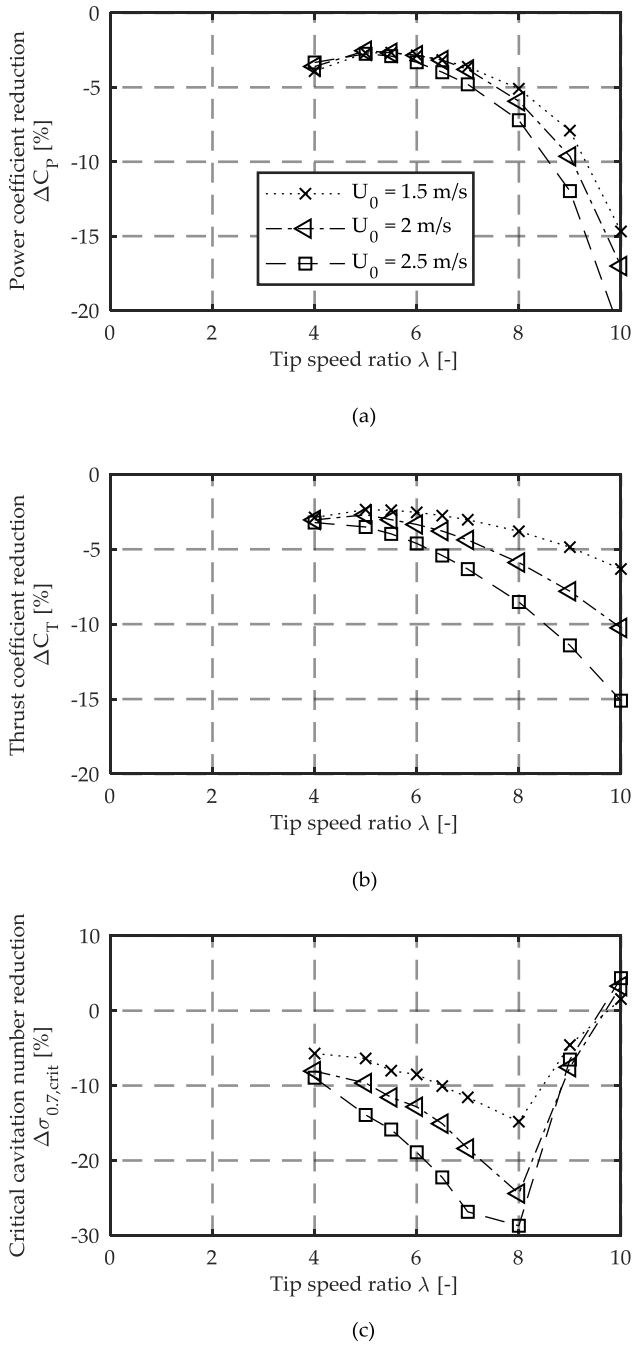

Fig. 10 Predicted differences between the performance of a rigid and flexible rotor: (a) power coefficient, (b) thrust coefficient and (c) the critical cavitation number for three different inflow velocities U_0.

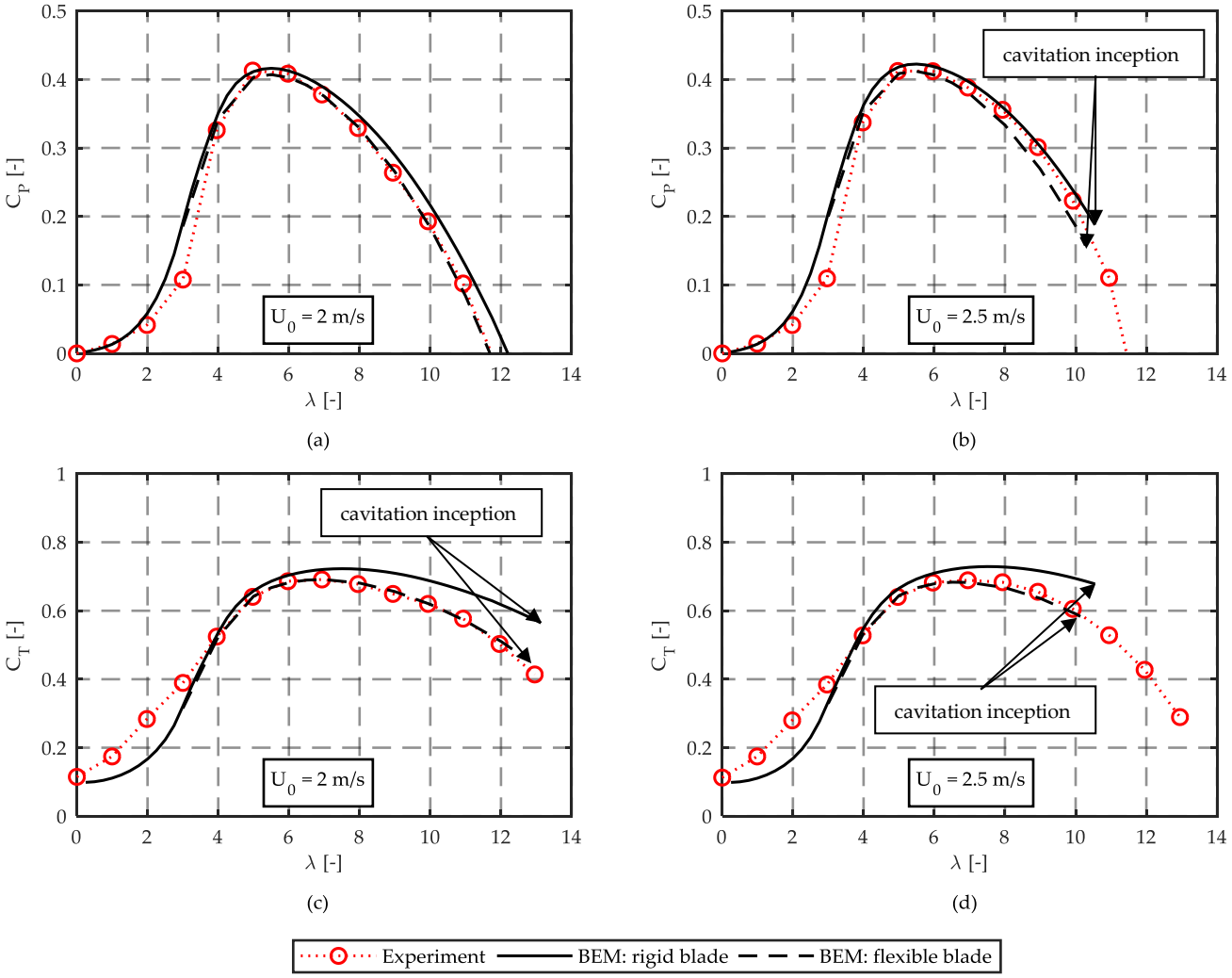

Fig. 11 BEM-predicted non-dimensional characteristics for different U_0 considering rigid blades (black solid line) and considering elastic deformation of the blades (flexible blade - dashed black line) and comparison with experimental data (towing tank).

VI. COMPARISON WITH EXPERIMENTAL RESULTS

Towing tank tests of the turbine were conducted for in-flow velocities of U_0 = 2 m/s and U_0 = 2.5 m/s. Measurements at higher inflow velocities were not possible because a significant deformation of the blades was observed. To avoid a plastic deformation and hence permanent damage of the blades in-flow velocity was limited to U_0 = 2.5 m/s.

Fig. 11 shows non-dimensional power and thrust characteristics, obtained from the towing tank tests. Additionally, the BEM prediction of C_P and C_T are plotted for a rigid rotor (black solid lines) and the predictions including the simulated elastic deformation of the blades due to the acting loads, i.e. the flexible rotor (black dashed lines). The BEM predictions are solely plotted for the non-cavitating operating points (according to the cavitation model).

The experimentally obtained power coefficients are in good agreement with the BEM predictions for the stall free operating range, i.e. $\lambda \geq 4$. A distinct statement which C_P prediction is more accurate is hardly possible. For the lower U_0 the flexible prediction seems to be more accurate whereas it is vice versa for U_0 = 2.5 m/s. In contrast, the thrust coefficients for rigid blades are significantly higher as the experimentally obtained data for $\lambda \geq 4$. The predicted C_T values of the flexible blades are in very good agreement with the experimentally obtained predictions for $\lambda \geq 4$. This implies that the observed deformation of the blades during the towing tank tests results in reduced thrust loads compared to the originally predicted values of the (rigid) turbine design. The differences of the performance predictions, rigid and flexible, to the experimentally obtained data for the operating range $\lambda < 4$ displaying the limitations of the VITERNA model for stalled hydrofoil sections.

Summarizing, the design of the stacking line aiming for a high pitching moment as well as the good agreement of the BEM prediction considering FEM simulated deformation imply that the significant deviation of the originally predicted C_T and experimentally obtained thrust coefficients are caused by the load related deformation of the blades. Furthermore, the potential of flexible blades to reduce the thrust is displayed. Nevertheless, stiff blades are favorable for experiments to validate the original

hydrodynamic turbine design since the deformation adds an element of uncertainty.

To avoid damages of the blades, the cavitation tunnel tests were conducted at U_0 = 1.5 m/s since the high blockage ratio (27%) increases the loads compared to the towing tank tests (cp. BAHAJ et al. [21]). Due to the low U_0 it was not possible to decrease the cavitation number far enough to visually observe cavitation types other than tip vortex cavitation at a sufficient operating range. Instead, a significant drop of the power coefficient is taken as an undesired phenomenon related to cavitation to define $\sigma_{0.7,crit}$. Moreover, the cavitation related reduction of the power output is of a high practical relevance since it reduces the energy yield of the turbine. **Fig. 13** shows the change of the C_P for decreasing cavitation numbers relative to the C_P at the highest $\sigma_{0.7}$ exemplarily for λ = 6. For a constant operating point, the pressure is reduced continuously starting at non-cavitating operation. The turbine is observed visually to detect cavitation as well as a display of the instant power output of the turbine. To take the measurements, shown in **Fig. 13,** the pressure is kept constant at regular intervals and the turbine performance is recorded. As soon as cavitation at the turbine or a significant power drop is observed an additional measurement is conducted.

In **Fig. 12** the experimentally obtained critical cavitation numbers regarding the onset of tip vortex cavitation attached to the blade and the onset of a reduced power output are plotted as function of the tip speed ratios and compared to the BEM predicted $\sigma_{0.7,crit}$ curves. Since the results of the towing tank measurements discussed above imply that the blades are deformed by the acting loads, $\sigma_{0.7,crit}$ is predicted for the rigid geometry and a flexible rotor. At the investigated operating range, the tip vortex cavitation incepts at higher $\sigma_{0.7}$ as compared to the onset of the power loss. The simulated deformation of the blades obviously results in a shift of the predicted $\sigma_{0.7,crit}$ curve towards lower tip speed ratios. The BEM model somewhat overpredicts the experimentally identified cavitation inception for rigid as well as flexible blades. The consideration of the simulated blade deformation provides a reduced overall deviation. However, the BEM model yields a conservative estimate of the onset of cavitation related power loss.

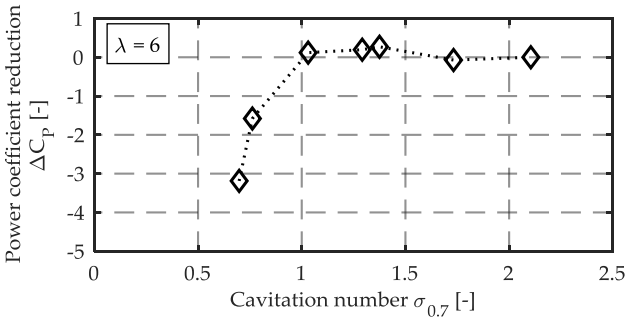

Fig. 13 Change of the power coefficient for decreasing cavitation numbers relative to the start value (highest $\sigma_{0.7}$) at λ = 6 and U_0 = 1.5 m/s..

VII. SUMMARY AND CONCLUSIONS

The objective of this contribution was a numerical and experimental assessment of the torsion-related performance change of a 1:12.6 brass model from a 6.3 m fixed pitch horizontal axis tidal turbine. Therefore, a BEM model is coupled to an FEM model and solved iteratively.

It was found that the axial bending of the blades was accompanied by a distinctive torsion which led to increased pitch angels. Comparing the performance predictions for the rigid and flexible rotor blades showed that the obtained variation in pitch angle distribution led to i) a decreased power output, ii) considerably reduced thrust loads and iii) somewhat lower critical cavitation numbers for a wide operating range. Thus, the numerical results imply that the blades - with isotropic material properties - experience a performance affecting torsion.

Experimental performance characteristics of the -

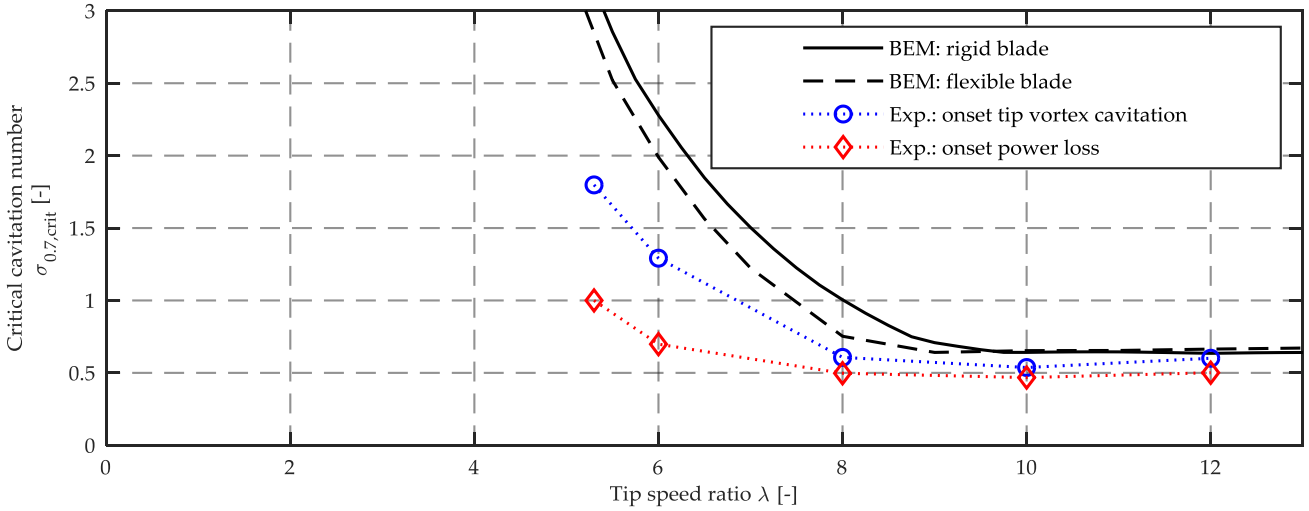

Fig. 12 BEM-predicted critical cavitation numbers for rigid blades (black solid line) and flexible blades (black dashed line) compared to the experimentally obtained critical cavitation numbers regarding the onset of tip vortex cavitation (blue circles) and the onset of power loss (red diamonds).

unavoidably flexible - model scale turbine were obtained in comprehensive towing tank and cavitation tunnel tests. A comparison with the prediction strongly suggests, that the model-scale turbine experienced the deformation as obtained from the FEM. Measurements with turbine model which experiences no deformation are needed to evaluate performance of rigid blades and hence the original blade design.

Acknowledgment

This work was founded by the Federal Ministry for Economic Affairs and Energy of Germany (BMWi) within the project TIDAL POWER (FKZ: 0325817B).

References

[1] P. Jeffcoate, R. Starzmann, B. Elsaesser, S. Scholl, and S. Bischoff, "Field measurements of a full scale tidal turbine," *International Journal of Marine Energy*, vol. 12, pp. 3–20, 2015.

[2] R. Starzmann, I. Goebel, and P. Jeffcoate, "Field Performance Testing of a Floating Tidal Energy Platform - Part 1: Power Performance," in *Proceedings of the 4th Asian Wave and Tidal Energy Conference*, 2018.

[3] R. Starzmann, M. Baldus, E. Groh, N. A. Lange, and S. Scholl, "Full-Scale Testing of a Tidal Energy Converter Using a Tug Boat," in *Proceedings of the 10th European Wave and Tidal Energy Conference*, Aalborg, Denmark, 2013.

[4] N. Kaufmann, "Small Horizontal Axis Free-Flow Turbines for Tidal Currents," Dissertation, Universität Siegen, submitted December 2018.

[5] R. F. Nicholls-Lee, S. R. Turnock, and S. W. Boyd, "Application of bend-twist coupled blades for horizontal axis tidal turbines," *Renewable Energy*, vol. 50, pp. 541–550, 2013.

[6] M. Motley and R. B. Barber, "Passive control of marine hydrokinetic turbine blades," *Composite Structures*, vol. 110, pp. 133–139, 2014.

[7] R. Barber, C. Hill., P. Babuska, M. Somoano, R. Wiebe, A. Aliseda and M. Motley, "Adaptative pitch marine hydrokinetic turbine blades: experimental loading, performance and wake imaging," 36th International Conference on Ocean, Offshore and Arctic Engineering, ASME 2017.

[8] R. Murray, T. Nevalainen, K. Gracie-Orr, D. Doman, M. Pegg and C. Johnstone., "Passively adaptive tidal turbine blades: Design tool development and initial verification," *International Journal of Marine Energy*, 2016.

[9] R. E. Murray,S. Ordonez-Sanchez, K. Porter, D. Doman, M. Pegg and C. Johnstone., "Towing tank testing of passively adaptive composite tidal turbine blades and comparison to design tool," *Renewable Energy*, vol. 116, pp. 202–214, 2018.

[10] N. Kaufmann, T. H. Carolus, and R. Starzmann, "Multi-Objective Optimization of Blades for Fixed-Pitch Horizontal Axis Tidal Stream Turbines with Variable Speed Control," in *Proceedings of the 12th European Wave and Tidal Energy Conference*, Cork, Ireland, 2017.

[11] N. Kaufmann, T. H. Carolus, and R. Starzmann, "An enhanced and validated performance and cavitation prediction model for horizontal axis tidal turbines," *International Journal of Marine Energy*, vol. 19, pp. 145–163, 2017.

[12] M. L. Buhl, "New Empirical Relationship between Thrust Coefficient and Induction Factor for the Turbulent Windmill State," Technical Report: NREL/TP-500-36834, National Renewable Energy Laboratory, Golden, CO, 2005.

[13] H. Glauert, "Airplane Propellers," in *Aerodynamic Theory: A General Review of Progress Under a Grant of the Guggenheim Fund for the Promotion of Aeronautics*, W. F. Durand, Ed., Berlin, Heidelberg: Springer Berlin Heidelberg, 1935, pp. 169–360.

[14] W. Z. Shen, R. Mikkelsen, J. N. Sørensen, and C. Bak, "Tip loss corrections for wind turbine computations," *Wind Energ.*, vol. 8, no. 4, pp. 457–475, 2005.

[15] M. Drela, *XFoil - Subsonic Airfoil Development System*, 2013.

[16] M. Drela, "Implicit Implementation of the Full e^n Transition Criterion," in *21st AIAA Applied Aerodynamics Conference*, Orlando, Florida, 2003.

[17] L. A. Viterna and R. D. Corrigan, "Fixed Pitch Rotor Performance of Large Horizontal Axis Wind Turbines," in *DOE/NASA Workshop on Large Horizontal Axis Wind Turbines*, Cleveland, 1981.

[18] Deutsches Kupferinstitut, *Datenblatt - CuZn39Pb2.* [Online] Available: https://www.kupferinstitut.de/fileadmin/user_upload/kupferinstitut.de/de/Documents/Shop/Verlag/Downloads/Werkstoffe/Datenblaetter/Messing/CuZn39Pb2.pdf. Accessed on: Nov. 22 2018.

[19] International Towing Tank Conference, *Testing and Extrapolation Methods Propulsion, Propulsor Open Water Test*, ITTC 7.5-02-03-02.1, 2002.

[20] International Towing Tank Conference, *Testing And Extrapolation Methods Propulsion Cavitation - Model Scale Cavitation Test*, ITTC 7.5-02-03-03.1, 2002.

[21] A. S. Bahaj, A. F. Molland, J. R. Chaplin, and W. Batten, "Power and thrust measurements of marine current turbines under various hydrodynamic flow conditions in a cavitation tunnel and a towing tank," (en), *Renewable Energy*, vol. 32, no. 3, pp. 407–426, 2007.